Nonzero spectral gap in several uniformly spin-2 and hybrid spin-1 and spin-2 AKLT models

Wenhan Guo, Nicholas Pomata, and Tzu-Chieh Wei

C. N. Yang Institute for Theoretical Physics and Department of Physics and Astronomy, State University of New York at Stony Brook, Stony Brook, New York 11794-3840, USA

(Received 30 December 2020; revised 15 February 2021; accepted 16 February 2021; published 19 March 2021)

Recently a few 2D AKLT models have been shown to be gapped, including the one on the hexagonal lattice, whose local spin magnitude is spin-3/2. Here we report the existence of a nonzero spectral gap on several nontrivial AKLT models having either solely spin-2 or mixed spin-2 and spin-1 degrees of freedom. The hybrid models we consider are defined on the 3D diamond and 2D kagome lattices, where lattice sites are spin-2 and one single spin-1 degree of freedom is added on some or all of the edges. Although the spectral gap problem for the uniformly spin-2 AKLT models on the diamond, kagome, and square lattices is still open, we are able to establish the existence of the gap for spin-2 AKLT models on two planar lattices, which we call the inscribed square lattice and the triangle-octagon lattice, respectively. So far these latter two are the only two uniformly spin-2 AKLT models that have a provable nonzero gap above the ground state. We also discuss some attempts to prove the gap existence on both the square and kagome lattices. In addition, we show that if one can show that the gap of a finite-size, weighted AKLT Hamiltonian is larger than a certain threshold, then the original AKLT model on the square lattice is gapped in the thermodynamic limit. The threshold of the gap we obtain scales inversely with the linear size of the problem.

DOI: 10.1103/PhysRevResearch.3.013255

I. INTRODUCTION

The spin models constructed by Affleck, Kennedy, Lieb, and Tasaki (AKLT) in 1987 [1,2] have prompted many further developments. These include symmetry-protected topological phases [3–5], where the spin-1 AKLT chain notably exemplifies the one-dimensional Haldane phase [6] and the two-dimensional spin-2 model realizes Haldane's 2D disordered phase [7]. One key property for such phases of matter to be stable is the existence of a nonzero energy gap above the ground state. In one dimension, this was already solved in the original AKLT work [1] and general methods have been proposed and successfully applied [1,8,9]. Another, unexpected development in the study of AKLT states is their application to quantum computation [10–16]. In particular, certain two-dimensional AKLT states can be used under local measurements as a resource for universal quantum computation [12–16]. The existence of a gap would be useful to ensure that the ground state can be efficiently created by cooling a system under the engineered Hamiltonian.

AKLT's original conjecture, that the spin-3/2 AKLT model on the hexagonal/honeycomb lattice has a nonzero spectral gap, was proved recently in Refs. [17,18]. These two works analytically reduced different gap criteria and numerically verified them beyond any doubt. In Ref. [17] the existence of a nonzero gap was also demonstrated for other 2D degree-3 lattices (with uniformly spin-3/2 degrees of freedom) and two singly decorated ones (spin-1 mixed with, respectively, spin-3/2 and spin-2). But no AKLT models with uniformly spin-2 degrees of freedom in two or higher dimensions have yet been shown to be gapped in the thermodynamic limit. Here, we employ the method of Ref. [17] to several other AKLT models on: (1) the 3D singly decorated diamond lattice (mixed spin-2 and spin-1; see Fig. 1), (2) two 2D decorated kagome lattices (also mixed spin-2 and spin-1; see Fig. 2), (3) the 2D triangle-octagon lattice (see Fig. 3), and (4) the 2D 'inscribed square lattice' (see Fig. 4), with the latter two being uniformly spin-2.

Reference [19] was the first to discuss the problem of the gap on decorated honeycomb lattices, and proved the existence of the gap when the number n of decorations on each edge is 3 or greater. Similar decorated lattices for the AKLT models were also discussed previously in the context of measurement-based quantum computation in Ref. [15]. Extending the work of Ref. [19] to other lattices, Ref. [20] reduces the gap issue for multiply decorated ($n \geqslant 2$) lattices to a problem involving two original lattice sites and incident edges with decoration. This can be solved without the knowledge of nearby local geometry, be the undecorated lattice two-dimensional, three-dimensional, or even higher. This result implies that AKLT models on these decorated lattices are gapped in general. The unresolved problem of *singly* decorated lattices, with $n = 1$, may require the knowledge of nearby geometry, as demonstrated in the 2D singly decorated square lattice and hexagonal lattice [17]. They are the variant closest to the AKLT model on the original (undecorated) lattices.

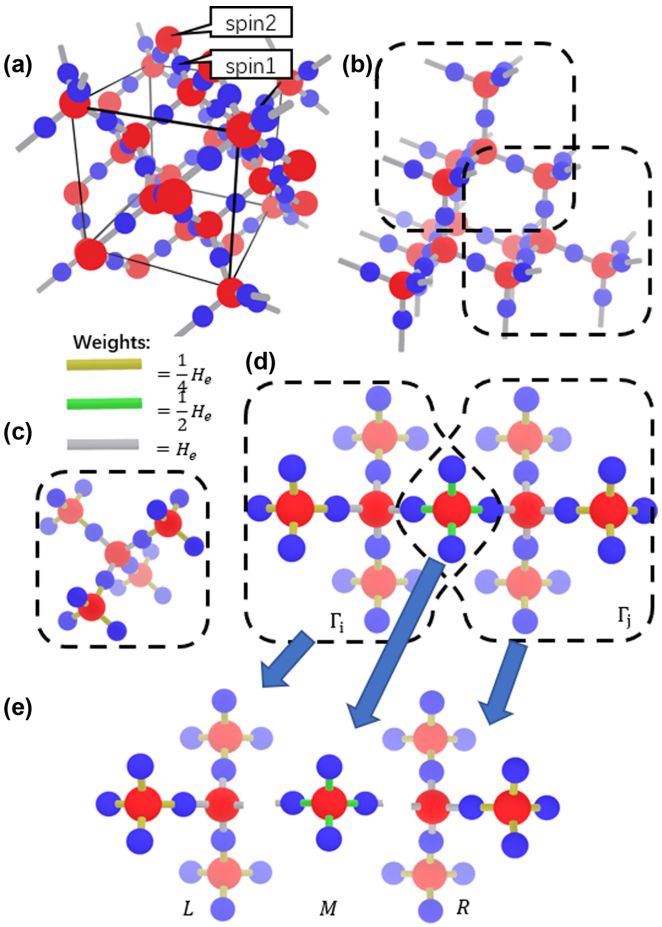

FIG. 1. (a) The decorated diamond lattice. (b) The overlapping scheme. (c) The subgraph Γ. (d) A pair of overlapping subgraphs. (e) The three parts of this pair of overlapping subgraphs.

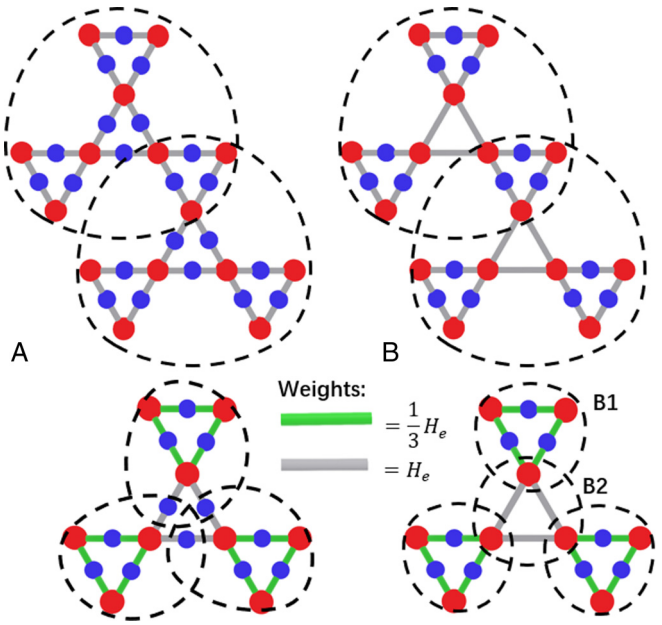

FIG. 2. The scheme for calculating the lower bound of two types of decorated kagome lattices: (A) uniformly decorated and (B) half-decorated. Also shown is the partition used to bound the gap of the respective subpatch.

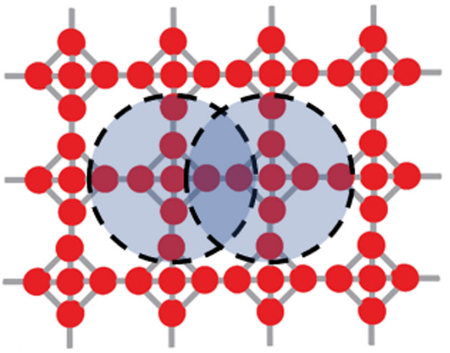

FIG. 3. The triangle-octagon lattice and the proposed overlapping scheme.

The spin-2 AKLT model on the original, undecorated diamond lattice is known to be disordered [21], but a sufficient condition for this to hold is the existence of a nonzero gap above the ground state, which is still evasive at the moment. The related singly-decorated model, with a single spin-1 entity added to every edge of the diamond lattice, is also likely to be disordered as the spin-1 decoration is likely to have larger quantum fluctuations than the spin-2 degrees of freedom, which may suppress any magnetic order. Here, we show that this decorated model is indeed gapped, demonstrating that the disordered nature of the model is stable against small perturbations. We also provide several different approaches for lower-bounding the energy gap, one of which yields $\Delta_{\text{lower}} \geqslant 0.013622$, which is still likely much lower than the actual gap.

The existence of a nonzero spectral gap in the spin-2 AKLT model on the kagome lattice is also not yet proved. We thus consider decorating the kagome lattice in two different ways, as illustrated in Fig. 2, where we have a spin-1 decoration (A) on every edge between neighboring spin-2 sites and (B) on only half of the edges. These two models are also shown to be gapped.

Additionally, we are able to establish the existence of a nonzero gap for AKLT models on two planar lattices where every site has spin 2, which we call the inscribed square lattice and the triangle-octagon lattice, respectively. Despite these results, we are still not able to prove a nonzero gap for

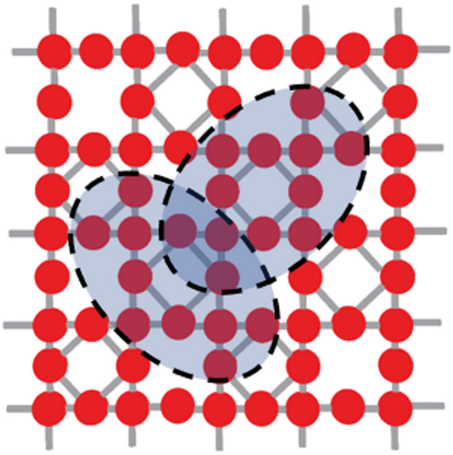

FIG. 4. The inscribed square lattice and the overlapping scheme.

the square lattice and the kagome lattice, but we discuss a few possible approaches to achieve that goal. Additionally, by using the approach introduced in Ref. [18], we also provide a finite-size criterion for the square lattice. We show that if one can determine that the gap of a weighted, finite-size AKLT Hamiltonian is larger than a certain threshold, then the AKLT Hamiltonian on the square lattice is gapped in the thermodynamic limit. This gap threshold scales inversely with the linear size of the problem. This means that if numerical methods, such as DMRG or other tensor network methods, could demonstrate a gap larger than the threshold for a certain size, then the issue of the AKLT gap on the square lattice would be solved. The remainder of the paper is organized as follows. In Sec. II, we review the method of proving the gap and provide more detailed discussions on how to obtain the lower bound on the energy gap. Different approaches for lower-bounding the gap are presented. In Sec. III, we give our results demonstrating the nonzero gap of the AKLT models on the singly decorated diamond lattice, two decorated kagome lattices, and two other planar lattices. In Sec. IV, we describe our attempts and ideas to tackle the gap problem on the kagome and square lattices. In Sec. V, we generalize the finite-size method in Ref. [18] and derive a corresponding criterion for establishing the gap in the AKLT model on the square lattice. We conclude in Sec. VI.

II. KEY METHODS

Following the procedure developed in Refs. [17,20], we first partition the graph (corresponding to the lattice in question) into overlapping subgraphs, which collectively contain all the edges. The original AKLT Hamiltonian can then be rearranged according to these subgraphs, with a suitable weight for each edge. We can use projectors supported on these subgraphs to construct a Hamiltonian that lower bounds the original AKLT Hamiltonian. If such a lower-bounding Hamiltonian can be shown to be gapped, then the original AKLT Hamiltonian is gapped and a lower bound on the gap may also be obtained. Examples of these partitions for degree-3 Archimedean lattices were found in Ref. [17], and those for the five models shown to be gapped in this work are shown in Figs. 1–4.

There are multiple choices of subgraphs, with no generic approach to determine which one to successfully prove a nonzero gap. It is thus necessary to check explicitly whether the gap criterion is satisfied. We shall discuss this criterion below; but, in brief, it reduces to an eigenvalue problem for a sum operator supported on two overlapping subgraphs; see Eqs. (5) and (6) below. However, even for two subgraphs with relatively small sizes, the corresponding Hilbert space may have too large a dimension to diagonalize on any computer. The tensor-network method introduced in Ref. [17] will be used to reduce the problem size substantially, and if it becomes solvable on a computer, the gap criterion can be verified with high precision.

A. Lower-bounding the Hamiltonian using projectors

Given a set of subgraphs Γ_i, the AKLT Hamiltonian can be rearranged as the sum of weighted AKLT Hamiltonian on each subgraph,

$$H_{\mathrm{AKLT}} = \sum_e H_e = \sum_i \sum_{e\in\Gamma_i} w_e^{(\Gamma_i)} H_e. \tag{1}$$

We then bound the subgraph AKLT Hamiltonian H_{Γ_i} with the orthogonal projector $\tilde{H}_i$ that has the same ground space as H_{Γ_i},

$$H_{\Gamma_i} = \sum_{e\in\Gamma_i} w_e^{(\Gamma_i)} H_e \geqslant \gamma_0 \tilde{H}_i, \tag{2}$$

where γ_0 is the least nonzero eigenvalue of H_{Γ_i}.

B. Gappedness and gap lower bound

If we can prove the lower-bounding Hamiltonian $\tilde{H} = \sum_i \tilde{H}_i$ has a gap $\tilde{\gamma}$, i.e.

$$\tilde{H}^2 \geqslant \tilde{\gamma}\tilde{H}, \tag{3}$$

then the AKLT Hamiltonian is gapped. To do this, we consider contributions to $\tilde{H}^2$. Since nonoverlapping pairs of Hamiltonian terms commute, we can thus discard these positive semi-definite terms, yielding a lower bound on $\tilde{H}^2$,

$$\tilde{H}^2 = \sum_i \tilde{H}_i + \sum_{i\neq j} \tilde{H}_i\tilde{H}_j \tag{4a}$$

$$\geqslant \tilde{H} + \sum_{\langle i,j\rangle} \{\tilde{H}_i, \tilde{H}_j\} \geqslant (1-\tilde{z}\eta)\tilde{H}, \tag{4b}$$

where $\langle i, j\rangle$ denotes a pair of neighbors that overlap, $\tilde{z}$ is the number of neighbors that subgraph Γ_i overlaps, and η is the overlapping parameter defined in Eq. (6) below, which measures how much the anticommutator can contribute negatively. We will discuss below in detail how to determine η.

Importantly, if $1-\tilde{z}\eta > 0$, then $\tilde{H}$ is gapped and so is the original AKLT Hamiltonian. In terms of Eq. (3), we can take $\tilde{\gamma} = 1-\tilde{z}\eta > 0$, and, combining with γ_0, we find a lower bound on the gap of the original AKLT Hamiltonian,

$$\Delta_{\mathrm{lower}} = \gamma_0(1-\tilde{z}\eta). \tag{5}$$

C. Reducing the gap criterion to an eigenvalue problem

From the above discussion, we know that $\eta < 1/\tilde{z}$ guarantees the existence of the gap. It is thus important to discuss the property η, defined as the greatest possible negative contribution the cross-term of overlapping subgraphs can make, i.e.,

$$\{\tilde{H}_i, \tilde{H}_j\} \geqslant -\eta(\tilde{H}_i + \tilde{H}_j). \tag{6}$$

For convenience, we define $E = \mathbb{1} - \tilde{H}_i$, $F = \mathbb{1} - \tilde{H}_j$ as the complements of the subgraph projectors. Equation (6) holds if and only if the following holds:

$$\{E, F\} \geqslant -\eta(E+F), \tag{7}$$

as proved in Refs. [9,20]. Geometrically, η is the cosine of the least nontrivial angle between the hyperplanes corresponding to the two projectors E and F, and $1\pm\eta$ is the greatest or, respectively, least noninteger eigenvalue of $E+F$. This can be shown by considering an eigenvector w. If we exclude the subspaces $\ker E \bigcap \ker F$ and $\ker E^\perp \bigcap \ker F^\perp$, which correspond to eigenvalues 0 and 2, respectively, then there is a unique decomposition of any vector w into two vectors $w =$

$u+v$, with u and v lying in $\ker F^\perp$ and $\ker E^\perp$, respectively. If w is an eigenvector of $E+F$, the two vectors u and v in the decomposition obey [20]

$$Eu = u, Ev = -\alpha u \tag{8a}$$

$$Fv = v, Fu = -\alpha v, \tag{8b}$$

where $\alpha \in [-1, 1]$ is related to the eigenvalues of $E+F$ and $\{E, F\}$ by

$$(E+F)(u+v) = (1-\alpha)(u+v), \tag{9a}$$

$$(EF+FE)(u+v) = -\alpha(E+F)(u+v). \tag{9b}$$

Since $1 \pm \alpha$ gives all the noninteger eigenvalues of $\tilde{H}_i + \tilde{H}_j = 2\mathbb{1} - E - F$, by comparing (9) with the definition of η, we have

$$\eta = \sup_{\alpha \notin \mathbb{Z}} |\alpha|, \tag{10}$$

which was proven in Ref. [20].

D. Projecting the problem into a lower-dimensional subspace

For an overlapping pair of subgraphs Γ_i and Γ_j, we split their union into three subgraphs $\Gamma_L \equiv \Gamma_i \setminus \Gamma_j$, $\Gamma_M \equiv \Gamma_i \bigcap \Gamma_j$, and $\Gamma_R \equiv \Gamma_j \setminus \Gamma_i$. The noninteger eigenvectors of $E+F$ are in the subspace spanned by the tensor products of ground states of the local AKLT Hamiltonians for Γ_L, Γ_M, and Γ_R, so we can perform the diagonalization on a smaller "virtual" space.

To understand this, we denote by A_L, A_M, and A_R the projectors onto the ground space of the AKLT Hamiltonian for Γ_L, Γ_M, and Γ_R, respectively. Without loss of generality, we consider $A = A_L$, satisfying [17,20]

$$EA = AE = E, \tag{11a}$$

$$FA = AF. \tag{11b}$$

The first equation comes from the frustration freeness of AKLT Hamiltonians and $\Gamma_A \subset \Gamma_i$. The second comes from $\Gamma_A \bigcap \Gamma_j = \emptyset$. Then for an eigenvector $w = u + v$ of $E+F$ with a noninteger eigenvalue (and hence $\alpha \neq 0$), the projector A preserves w,

$$Aw = \alpha^{-2} AFEw = \alpha^{-2} FAEw = \alpha^{-2} FEw = w. \tag{12}$$

Hence, A_L, A_M, and A_R preserve the noninteger spectrum of $E+F$. We can thus find an orthonormal basis which spans the image of $A_L \otimes A_M \otimes A_R$.

E. Constructing the projectors using tensor networks

There is an isometry that maps the ground space of the AKLT Hamiltonian on a subgraph to the "virtual-space" representation which consists of virtual-spin degrees of freedom for each vertex with free edges [17,20]. Thus, there is a "holographic" correspondence for the ground space from the physical spins on the bulk to the virtual spins on the boundary. Our goal is to replace the physical indices in the projectors E and F by virtual indices on the boundaries of the subgraphs Γ_L, Γ_M, and Γ_R. This makes it possible to numerically solve a diagonalization problem when the original physical dimension is much too large for diagonalization to be tractable. We emphasize that the reduction, though done numerically via the singular value decomposition (SVD), is exact in principle.

This isometry is built out of the AKLT tensor Ψ_Γ, which can be written in terms of a tensor network. The basic building blocks of the tensor network are the following.

(1) For each vertex a with degree z_a, an isometry $P_a^{[z_a/2]}$, which maps the total symmetric space of z_a virtual spin-1/2 (with basis states labeled by $\uparrow$ and $\downarrow$) to the physical spin-$z_a/2$ space. The expressions for a degree-2 vertex and a degree-4 vertex are, respectively,

$$P_a^{[1]} = |1\rangle\langle\uparrow\uparrow| + |0\rangle \frac{1}{\sqrt{2}}(\langle\uparrow\downarrow| + \langle\downarrow\uparrow|) + |-1\rangle\langle\downarrow\downarrow|, \tag{13a}$$

$$\begin{aligned} P_a^{[2]} = {} & |2\rangle\langle\uparrow\uparrow\uparrow\uparrow| \\ & + |1\rangle \frac{1}{2}(\langle\uparrow\uparrow\uparrow\downarrow| + \langle\uparrow\uparrow\downarrow\uparrow| + \langle\uparrow\downarrow\uparrow\uparrow| + \langle\downarrow\uparrow\uparrow\uparrow|) \\ & + |0\rangle \frac{1}{\sqrt{6}}(\langle\uparrow\uparrow\downarrow\downarrow| + \langle\uparrow\downarrow\uparrow\downarrow| + \langle\downarrow\uparrow\uparrow\downarrow| \\ & + \langle\uparrow\downarrow\downarrow\uparrow| + \langle\downarrow\uparrow\downarrow\uparrow| + \langle\downarrow\downarrow\uparrow\uparrow|) \\ & + |-1\rangle \frac{1}{2}(\langle\uparrow\downarrow\downarrow\downarrow| + \langle\downarrow\uparrow\downarrow\downarrow| + \langle\downarrow\downarrow\uparrow\downarrow| + \langle\downarrow\downarrow\downarrow\uparrow|) \\ & + |-2\rangle\langle\downarrow\downarrow\downarrow\downarrow|. \end{aligned} \tag{13b}$$

(2) For each edge $e = (a, b)$, an antisymmetric tensor K which contracts with a pair of virtual spin-1/2's on each end of the edge,

$$K_e = \frac{1}{\sqrt{2}}(|\uparrow\rangle_a |\downarrow\rangle_b - |\downarrow\rangle_b |\uparrow\rangle_a). \tag{14}$$

These two elements combine to define the AKLT wave function, providing a natural expression of the wave function in terms of a tensor network; see, e.g., Fig. 5.

As illustrated in Fig. 5(h), if we contract all the vertex tensors and edge tensors, we can treat the resulting tensor as a matrix, with the "right side" being a fusion of uncontracted indices that correspond to virtual spins on the dangling edges of the subgraph, and the 'left side' being a fusion of indices corresponding to the physical spins on the vertices. However, this matrix is not full-rank, because for vertices with $z'_a > 1$ dangling edges, the vertex tensor only acts nontrivially on the totally symmetric subspace of the remaining z'_a spin-1/2s. We can "fix" it by further contracting the remaining z'_a virtual spins with $P'^{[z'_a/2]\dagger}_a$, which means that we replace these z'_a spin-1/2s with a spin-$z'_a/2$ degree of freedom. It was shown that such a counting is exact [17] and is a generalization of the uniqueness of the ground state in the AKLT model under appropriate boundary conditions [22].

Altogether we arrive at the AKLT tensor, as illustrated in Figs. 5(a)–5(c),

$$\Psi_\Gamma = \prod_{a\in\Gamma} P_a^{[z_a/2]} \prod_{e\in\Gamma} K_e \prod_{a\in\partial\Gamma} P'^{[z'_a/2]\dagger}_a. \tag{15}$$

This tensor $\Psi_\Gamma : \mathcal{H}_{\text{virtual}} \to \mathcal{H}_{\text{physical}}$ is an isometry from the virtual space to the AKLT ground subspace of the physical degrees of freedom. Therefore the ground subspace is the span

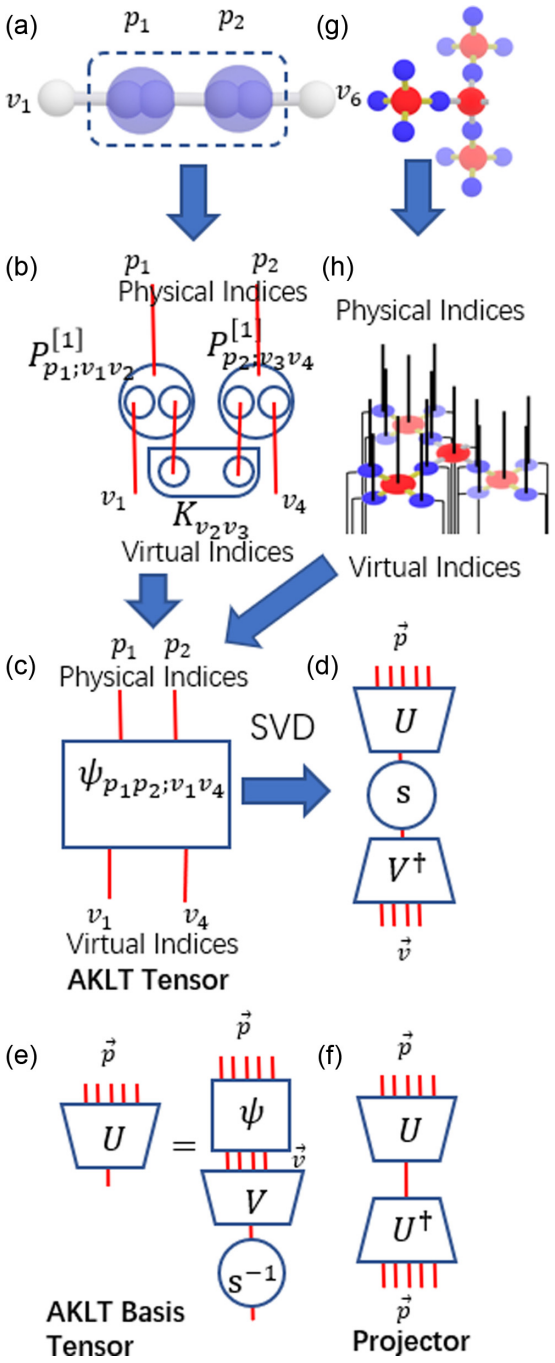

FIG. 5. Illustration of how to extract the projector to the AKLT ground space of an given region or subgraph. (a) A subgraph in a 1D AKLT chain is used as an example, where each physical spin can be written as symmetric sum of virtual spins. [(b) and (c)] The AKLT tensor $\Psi = UU^\dagger$ is constructed by applying symmetrizers P at each vertex to the tensor product of antisymmetric virtual spin doublet states K at each edge and external virtual spins at dangling edges. [(d) and (e)] The AKLT basis tensor U is the AKLT tensor, orthonormalized using a singular value decomposition $\Psi = UsV^\dagger$. To avoid storing tensors with large physical dimensions explicitly, s and V are calculated numerically from $\Psi^\dagger\Psi$. U is represented in terms of a tensor network as $U = \Psi V s^{-1}$. (f) The projector $\Pi = UU^\dagger$. [(g) and (h)] Another example of an AKLT Tensor on a more complicated subgraph.

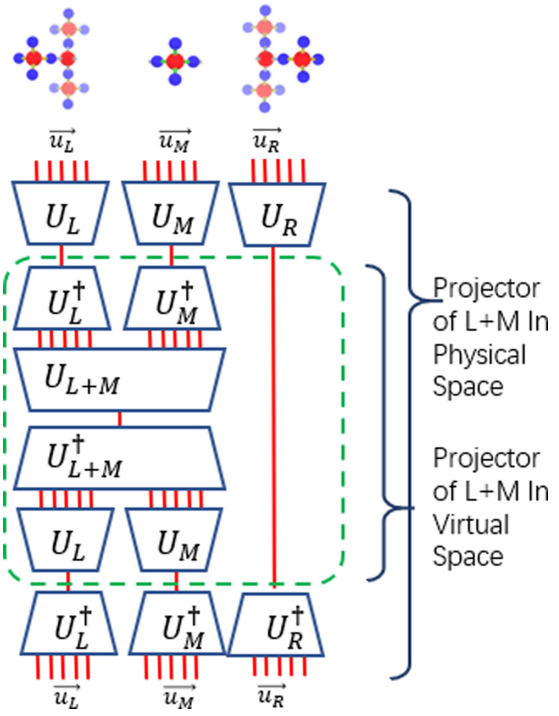

FIG. 6. We can reduce the dimension of the projector $E = U_{L+M}U_{L+M}^\dagger$ by using the fact that $A_L = U_L U_L^\dagger, A_M, A_R$ only annihilate eigenvectors of E with integer eigenvalue. Since U_L acts isometrically on the image of A_L, the noninteger eigenvalues of $E + F$ can be obtained by performing the spectral decomposition of tensors derived from the tensor in the dashed green box and the corresponding tensor for $M + R$.

of the left singular vectors of Ψ_Γ, which can be obtained from the singular value decomposition (SVD) of Ψ_Γ,

$$\Psi_\Gamma = U_\Gamma s_\Gamma V_\Gamma^\dagger, \tag{16a}$$

$$\Pi_\Gamma = U_\Gamma U_\Gamma^\dagger, \tag{16b}$$

where U_Γ is the orthonormalized AKLT tensor whose column vectors span the ground subspace of the AKLT Hamiltonian H_Γ; Π_Γ is the projector to the ground subspace.

To avoid the large physical dimension and to take advantage of the smaller virtual dimension, we can perform the SVD via the eigenvalue decomposition for $\Psi^\dagger\Psi$, which is a $\dim \mathcal{H}_v \times \dim \mathcal{H}_v$ matrix,

$$\Psi^\dagger\Psi = V_\Gamma s_\Gamma^2 V_\Gamma^\dagger. \tag{17}$$

Since U_Γ is a $\dim \mathcal{H}_p \times \dim \mathcal{H}_v$ matrix, which may be too large to fit in the computer memory, we express U_Γ from the tensor network representation of Ψ, as seen in Figs. 5(d) and 5(e),

$$U_\Gamma = \Psi_\Gamma V_\Gamma s_\Gamma^{-1}. \tag{18}$$

Using the tensor-network representations of $A_L = U_L U_L^\dagger, A_M, A_R, E$, and F, we can write the action of $(A_L \otimes A_M \otimes A_R)E$ and $(A_L \otimes A_M \otimes A_R)F$ by contracting the physical indices; see Fig. 6. To extract the noninteger eigenvalues, we can consider only the tensor inside the dashed box in Fig. 6. This reduces to studying the action of E

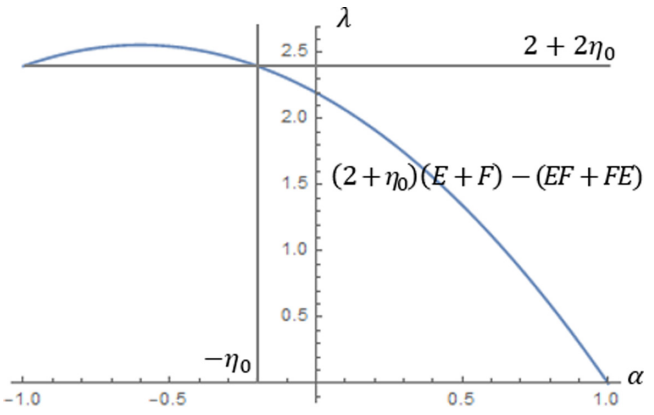

FIG. 7. The α vs λ plane, where α is as in (9) and λ is the eigenvalue of a quadratic polynomial of $E+F$, which we hope to choose such that eigenvectors with $\alpha \leqslant -\eta_0$ will yield an eigenvalue $\geqslant 2+2\eta_0$. Note that α is symmetrically distributed with respect to 0. Here $\eta_0 = 0.2$.

and F on the image of $A_L \otimes A_M \otimes A_R$, using the orthonormal basis $U_L \otimes U_M \otimes U_R$.

F. Methods to extract the largest noninteger eigenvalue

We use the standard ARPACK library to do the eigenvalue decomposition in Eq. (17) and sparse maximum-eigenvalue extractions of quadratic polynomials of $E+F$. Below, we mostly focus on the case where the size of $E+F$ (when reduced to virtual degrees of freedom) is large enough that it cannot be exactly diagonalized directly but is still small enough to extract the largest or smallest eigenvalues by the Lanczos method.

The tensor-network representations in (18) and Figs. 5, 6 are handled using a python package called TENSORNETWORK. The action of E on a vector $v \in \mathcal{H}_v$ is evaluated by contracting the tensor network representation of this expression. The path of contraction is calculated using the PYTHON package OPT_EINSUM, to ensure that the size of intermediate tensors does not exceed the memory limit.

Given the action of E and F, one can extract the spectrum using the iterative method provided in ARPACK. However, the size of the problem makes it only feasible to extract the first several greatest-magnitude eigenvalues. Thus we consider the quadratic polynomial of $E+F$:

$$O \equiv (2+\eta_0)(E+F) - (EF+FE). \tag{19}$$

The action of O on an eigenvector w is

$$Ow = (2+\eta_0+\alpha)(1-\alpha)w. \tag{20}$$

As illustrated in Fig. 7, our goal is to find $\eta = \sup_{\alpha\notin\mathbb{Z}} |\alpha|$, where the noninteger α's are symmetrically distributed around 0.

We first guess an η_0 and evaluate the largest eigenvalue λ of O. If λ is close to $2+2\eta_0$ up to numerical error, then we can almost claim that there is no noninteger $\alpha \gtrsim \eta_0$. In this case, the largest eigenvalue comes from $a=-1$ or $a \approx -\eta_0$. The approximation sign comes from numerical error. We can further exclude the second case by doing another calculation using a slightly smaller η_0'. If $\lambda' \approx 2+2\eta_0'$, then we know $\alpha = -1$. By decreasing η_0 carefully we finally find an η_0, where $\lambda - (2+2\eta_0)$ is large enough compared to the numerical error. Then, we have

$$\alpha = -\tfrac{1}{2}(1+\eta_0 \pm \sqrt{(\eta_0+3)^2 - 4\lambda}). \tag{21}$$

The $+$ branch is less than -1 and can be excluded, so

$$\eta = -\tfrac{1}{2}(1+\eta_0 - \sqrt{(\eta_0+3)^2 - 4\lambda}). \tag{22}$$

Importantly, if $1-\tilde{z}\eta > 0$, where $\tilde{z}$ is the number of overlapping neighbors of a subgraph, then the corresponding AKLT model has a nonzero spectral gap.

G. Evaluating the lower bound of the subgraph Hamiltonian gap

Having obtained the overlapping parameter η to verify the gap, the next step is to give a lower bound on the gap of the AKLT Hamiltonian via $\Delta_{\text{lower}} = \gamma_0(1-\tilde{z}\eta)$, where γ_0 is the gap of the weighted AKLT Hamiltonian on the subgraph Γ_i,

$$H_{\Gamma_i} = \sum_{e\in\Gamma_i} w_e H_e \geqslant \gamma_0 \tilde{H}_i. \tag{23}$$

The weights of the Hamiltonian term for a given edge in different subgraphs ums up to unity: $\sum_i w_e^{(\Gamma_i)} = 1$. We note that the weighted AKLT Hamiltonian on a finite graph is always gapped, since there are only finite number of eigenstates.

There are three ways to calculate the gap of this weighted AKLT Hamiltonian, which we now discuss.

1. The direct method

The ARPACK library contains a procedure to get the algebraically smallest eigenvalue given a sparse Hermitian linear operator. To calculate the gap, which is the second smallest eigenvalue above (with the smallest one being zero), we use the AKLT projector to shift the ground states to a higher level,

$$OP = \sum_{e\in\Gamma_i} w_e H_e + \left(\sum_{e\in\Gamma_i} w_e\right)\Pi_\Gamma. \tag{24}$$

Then we can apply ARPACK procedures to numerically calculate the smallest eigenvalue of the shifted Hamiltonian.

2. Lower bounding with sub-sub-graph projectors

For a larger subgraph to which one cannot apply the direct method, we decompose it further into sub-sub-graphs, which collectively contain all the edges in the subgraph, with weights on each edge summing up to the corresponding weight of the edge in the subgraph; see Fig. 8(a).

The weighted subgraph AKLT Hamiltonian is the sum of weighted AKLT terms in the sub-sub-graphs, which can each be lower-bounded by the sum of projectors orthogonal to the local ground state with appropriate weights (w_j'),

$$H_{\Gamma_i} = \sum_{\Gamma_j'} H_{\Gamma_j'} \geqslant \sum_{\Gamma_j'} w_j' \tilde{H}_{\Gamma_j'}, \tag{25}$$

where w_j' are the gaps of the Hamiltonian on the sub-sub-graphs, which can be calculated by method 1, and $\tilde{H}_{\Gamma_j'} = \mathbb{1}_{\Gamma_j'} - \Pi_{\Gamma_j'}$ is the projector onto the Hilbert space orthogonal

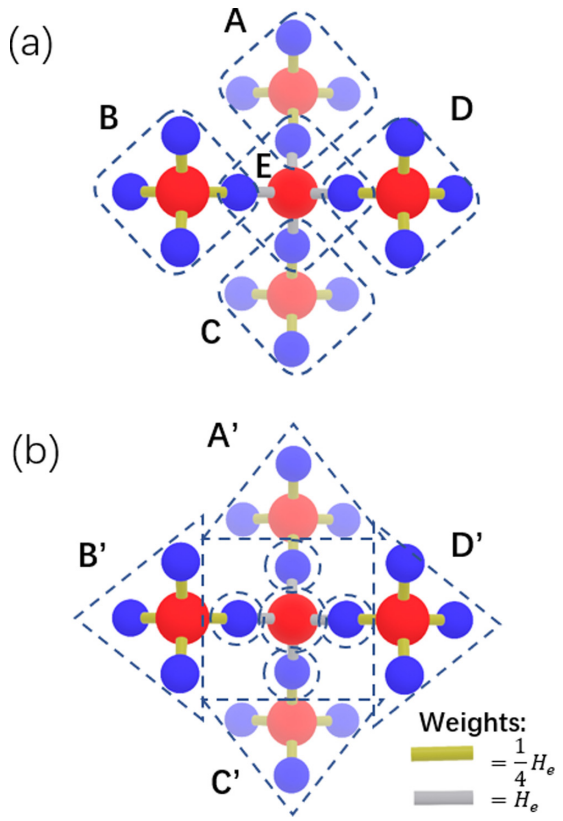

FIG. 8. Approach I for lower-bounding the gap. (a) The subgraph is decomposed into four overlapping regions. (b) An isometry will be applied to the nonoverlapping regions (the four triangular shapes A', B', C', and D') for dimensional reduction.

to the local ground state supported in the sub-sub-graph Γ'_j of subgraph Γ_i.

As in the reduction from physical to virtual degrees of freedom when we calculate the parameter η, we can project the Hamiltonian on the right-hand side (r.h.s.) of Eq. (25) to the virtual degrees of freedom and calculate its gap in order to bound the gap of the above H_{Γ_i}; see Fig. 8(b). This method was proposed in Section B of the Supplemental Materials of Ref. [17].

3. Overlapping sub-sub-graphs

In Eq. (25), we divide a subgraph Γ_i further into a few overlapping sub-sub-graphs Γ'_j. If these Γ'_j are chosen such that they are related by symmetry such as rotation, then the gap of their weighted AKLT Hamiltonians is identical, i.e., $w'_j = w$, yielding $H_{\Gamma_i} \geqslant w \sum_{\Gamma'_j} \tilde{H}_{\Gamma'_j}$. As in Eq. (3), we calculate the parameter η for $\sum_{\Gamma'_j} \tilde{H}_{\Gamma'_j}$, obtaining a lower bound on the gap of H_{Γ_i} of $w(1 - z\eta)$, where z denotes the number of overlapping neighbors of each sub-sub-graph Γ'_j. Of course, such a lower bound is meaningful only when $\eta < 1/z$.

III. RESULTS FOR FIVE AKLT MODELS

A. Decorated diamond lattice

We choose subgraphs Γ as in Fig. 1. Each Γ_i overlaps with $\tilde{z} = 12$ other Γ_j's in the same configuration. The virtual dimensions of $\Gamma_L = \Gamma_i \setminus \Gamma_j$, $\Gamma_M = \Gamma_i \bigcap \Gamma_j$, and $\Gamma_R = \Gamma_j \setminus \Gamma_i$ are 1024, 16, and 1024, respectively; their product is 16 777 216. The parameter η, determined from the largest noninteger eigenvalue $1 + \eta$ of the projector sum $E + F$, is calculated to be $\eta = 0.04131015388 < \frac{1}{12}$. This shows that the mixed spin-1/spin-2 AKLT model on the singly decorated diamond lattice has a nonzero gap in the thermodynamic limit.

We note that, in principle, our calculations are accurate to machine precision. However, in the following, we shall only present ten digits of accuracy, rounding the eleventh digit of η up and the eleventh digit of the gap estimate γ_0 down, such that the resulting value of Δ_{lower} in Eq. (5) is strictly a lower bound.

Next, we give two approaches to lower-bound the spectral gap of the AKLT Hamiltonian on the singly decorated diamond lattice.

1. First approach for a gap lower bound

Here we apply the method described in Sec. II G 2 to lower-bound the gap of an AKLT Hamiltonian. To do this, we consider the lower-bounding Hamiltonian $H_{\text{AKLT}} = \sum_i H_{\Gamma_i} \geqslant \gamma_0 \sum_i \tilde{H}_i$, where γ_0 is the gap of the weighted AKLT Hamiltonian H_{Γ_i} in a region Γ_i, and the lower bound of the AKLT gap is $\Delta_{\text{lower}} = \gamma_0(1 - \tilde{z}\eta)$. We will seek a lower bound on γ_0, as we cannot directly calculate its value, due to the excessive Hilbert-space dimension $3^{16}5^5$. We partition Γ_i into five overlapping sub-regions A, B, C, D, E, as illustrated in Fig. 8(a). We note that the weights in front of the local AKLT terms are 1 in sub-region E and 1/4 in all other sub-regions A-D. To lower-bound γ_0, we first lower-bound the Hamiltonian H_{Γ_i} via $H_{\Gamma_i} \geqslant \gamma_5[(\mathbb{1}_E - \Pi_E) + \sum_{j=A}^{D} \frac{1}{4}(\mathbb{1}_j - \Pi_j)] := \gamma_5 \tilde{H}_5$, where Π_j is the projector to the ground space in subregion j, and $\mathbb{1}_j$ is the identity operator supported on it. The gap of the AKLT Hamiltonian in each region is calculated to be $\gamma_5 = 0.17064623273$.

The second step is to bound the gap of $\tilde{H}_5$. Even though it has the same dimension as that of H_{Γ_i}, it consists of projectors on subregions. Therefore we can apply an isometry U_5, similar to those used in complexity reduction for calculating the parameter η, that consists of a product of isometric transformations on the four nonoverlapping subregions A', B', C', and D', shown in Fig. 8(b). This reduces the dimension of $\tilde{H}_5$ to that of $\tilde{H}'_5 \equiv U_5 \tilde{H}_5 U_5^\dagger$, which acts on a Hilbert space of dimension $2^{16} \times 3^4 \times 5$. Such a reduction allows us to use the Lanczos method to show the lowest nonzero eigenvalue of $\tilde{H}_5$ to be $\gamma_R = 0.15830084148$. As this number is smaller than the minimal weight 1/4 of the projectors in $\tilde{H}_5$, γ_R is a lower bound on the energy gap of $\tilde{H}_5$, following from proposition 5 in the Supplemental Material of Ref. [17]. Thus γ_0 is lower-bounded by $\gamma_0 \geqslant \gamma_5 \gamma_R \approx 0.027013442238$, and the lower bound on the gap of the AKLT Hamiltonian on the decorated diamond lattice is

$$\begin{aligned} \Delta_{\text{lower}} &\geqslant \gamma_0(1 - \tilde{z}\eta) \\ &= 0.013622288769. \end{aligned} \tag{26}$$

2. A second approach for the lower bound

Here we give an alternative to obtain the gap lower bound, described in Sec. II G 3. We first give the bound

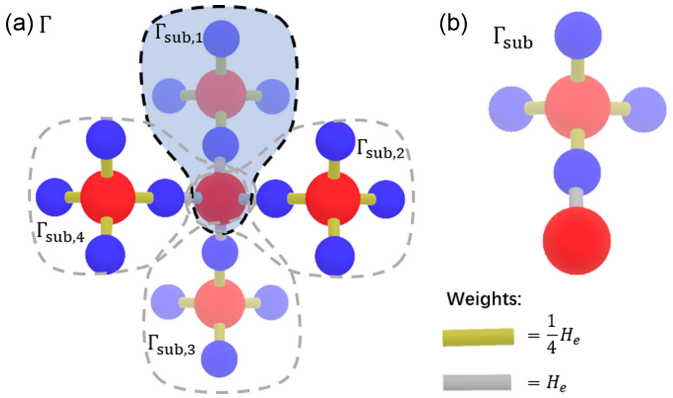

FIG. 9. Approach II for the gap lower bound via decomposing one subgraph Γ into four overlapping sub-sub-graphs.

obtained:

$$\begin{aligned}\Delta_{\text{lower}} &\geqslant \gamma_0(1-\tilde{z}\eta)\\ &\geqslant 0.013110607533\times(1-12\times 0.041310153882)\\ &= 0.0066113929572. \end{aligned} \tag{27}$$

As we explain above, the gap γ_0 of the AKLT Hamiltonian on a subgraph Γ of the decorated diamond lattice cannot be directly calculated. The second approach is to further decompose Γ into four overlapping sub-sub-graphs $\Gamma_{\text{sub},j}$; see Fig. 9(a). These four sub-sub-graphs are related to each other by rotating with respect to the center spin-2 site. We thus can lower-bound the Hamiltonian $H_\Gamma \geqslant \gamma_1 \sum_{j=1}^4 \tilde{H}_{\text{sub},j} := \gamma_1 \tilde{H}_{\text{sub}}$, where γ_1 is the gap of the weighted AKLT Hamiltonian in each region and $\tilde{H}_{\text{sub},j}$ is the projector onto the Hilbert space orthogonal to the local ground space. The physical dimension of each $\Gamma_{\text{sub},j}$ is $5^2 3^4 = 2025$, so we obtain the sub-sub-graph gap $\gamma_1 = 0.044374363959$ by exact diagonalization.

To obtain a lower bound on the gap of $\tilde{H}_{\text{sub}}$, we consider its square,

$$\begin{aligned}\tilde{H}_{\text{sub}}^2 \geqslant\ & \tilde{H}_{\text{sub},1}+\tilde{H}_{\text{sub},2}+\tilde{H}_{\text{sub},3}+\tilde{H}_{\text{sub},4}\\ &+\{\tilde{H}_{\text{sub},1},\tilde{H}_{\text{sub},2}\}+\{\tilde{H}_{\text{sub},1},\tilde{H}_{\text{sub},3}\}\\ &+\{\tilde{H}_{\text{sub},1},\tilde{H}_{\text{sub},4}\}+\{\tilde{H}_{\text{sub},2},\tilde{H}_{\text{sub},3}\}\\ &+\{\tilde{H}_{\text{sub},2},\tilde{H}_{\text{sub},4}\}+\{\tilde{H}_{\text{sub},3},\tilde{H}_{\text{sub},4}\} \qquad (28a)\\ \geqslant\ & (1-z_1\eta_1)\tilde{H}_{\text{sub}}, \qquad (28b)\end{aligned}$$

where the parameter η_1 is given by

$$\eta_1 = \sup_{\alpha\notin\mathbb{Z}} |\alpha|, \tag{29}$$

with α's defined by the eigenvalue equation

$$(\tilde{H}_{\text{sub},1}+\tilde{H}_{\text{sub},2})w = (1-\alpha)w. \tag{30}$$

Each $\Gamma_{\text{sub},i}$ overlaps with $z_1 = 3$ other $\Gamma_{\text{sub},j}$'s, with virtual dimensions $16\times 5\times 16 = 1280$. The parameter $\eta_1 = 0.23484848485$ is calculated using the method described above in Sec. II. Thus, we obtain a lower bound γ_0 on the gap of the subgraph Hamiltonian,

$$\begin{aligned}\gamma_0 &\geqslant \gamma_1(1-z_1\eta_1)\\ &= 0.044374363959\times(1\text{–}3\times 0.23484848485)\\ &= 0.013110607533. \end{aligned} \tag{31}$$

We also used three other approaches to lower bound the gap of the singly decorated diamond AKLT Hamiltonian. The results from all five different approaches (based on three different partitions of the Hamiltonian) are listed in Appendix A.

B. Two decorated kagome lattices

Here we consider two different types of decorated kagome lattices, in Fig. 2: one uniformly decorated (A) and the other half decorated (B). Each subgraph overlaps with $\tilde{z} = 6$ neighbors. The total virtual dimension $U_L \otimes U_M \otimes U_R$ acts on is $324\times 27\times 324 = 2\,834\,352$ for both cases.

It turns out that we can prove both models are gapped. For both cases, we have calculated the η parameter and estimated the corresponding lower bound on the gap. The results are $\eta_A = 0.061837628688$ and $\eta_B = 0.063876201589$. Both satisfy the criterion $1-\eta z > 0$, and both models are gapped.

Using the method described in Sec. II G 2, the lower bounds of the subgraph gaps $\gamma_{0,A}$ and $\gamma_{0,B}$ is calculated. The virtual dimensions are $27^3\times 3^3 = 531\,441$ for A, and $36^3\times 5^3 = 5\,832\,000$ for B, respectively. The gaps of the relevant sub-sub-graphs (see Fig. 2) are $\gamma_A = 0.087161682566$, $\gamma_{B1} = 0.27562963489$, and $\gamma_{B2} = 0.78571428572$. Thus the lower bound on the AKLT model on the subgraphs is obtained: $\gamma_{0,A} = 0.045113229196$ and $\gamma_{0,B} = 0.11856350721$.

Therefore we find lower bounds for these two AKLT models of, respectively,

$$\begin{aligned}\Delta_{\text{lowerA}} &= \gamma_{0,A}(1-\tilde{z}\eta_A)\\ &= 0.028375058500, \end{aligned} \tag{32}$$

$$\begin{aligned}\Delta_{\text{lowerB}} &= \gamma_{0,B}(1-\tilde{z}\eta_B)\\ &= 0.073123188281. \end{aligned} \tag{33}$$

C. Triangle-octagon lattice

We use the subgraph Γ, as shown in Fig. 3. Each Γ_i is overlapping with $\tilde{z} = 4$ other Γ_j's. The total virtual dimension $U_L \otimes U_M \otimes U_R$ acts on in this case is $512\times 16\times 512 = 4\,194\,304$. This configuration yields an $\eta = 0.22524594477 < \frac{1}{4}$.

The physical dimension of a single subgraph is $5^9 = 1\,953\,125$, which is small enough for exact diagonalization on the physical space. In practice, we adopt a shifted Hamiltonian $H_{\text{shifted}} = \sum_{e\in\Gamma} w_e H_e + (\sum_{e\in\Gamma} w_e)\Pi_\Gamma$, which shifts the ground state to an eigenvalue $\sum_{e\in\Gamma} w_e = 10$, much larger than the possible gap. As described in Sec. II G 1, we then calculate the gap by extracting the least eigenvalue of H_{shifted} using ARPACK, which gives $\gamma_0 = 0.09764599552$. The lower bound of the AKLT Hamiltonian on the triangle-octagon lattice is thus

$$\begin{aligned}\Delta_{\text{lower}} &= \gamma_0(1-\tilde{z}\eta)\\ &= 0.0096685374671. \end{aligned} \tag{34}$$

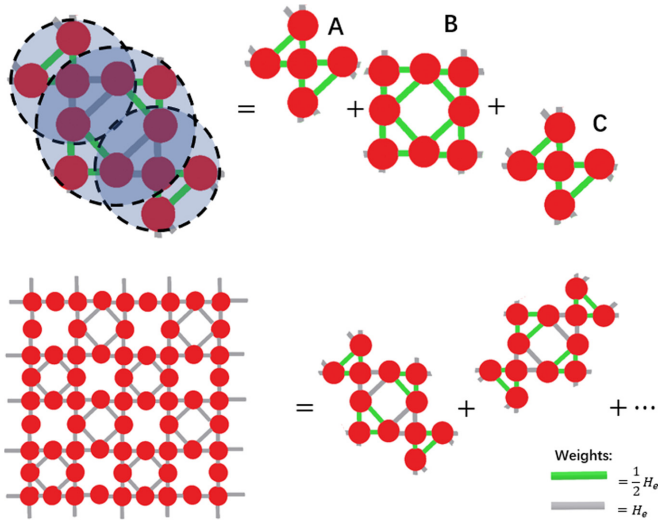

FIG. 10. The decomposition scheme of a subgraph of the inscribed square lattice. It also shows how the weights of the edges of sub-sub-graphs sum up to the weights in the subgraph, and the weights in the subgraphs sum up to 1 in the whole lattice.

D. Inscribed square lattice

We use the subgraph Γ in Fig. 4. Each Γ_i overlaps with $\tilde{z} = 4$ other Γ_j's with the same configuration. The total virtual dimension $U_L \otimes U_M \otimes U_R$ acts on in this case is $3888 \times 27 \times 324 = 34\,012\,224$. The result is $\eta = 0.20517748800 < \frac{1}{4}$.

We further decompose the subgraph according to Fig. 10. The gaps of sub-sub-graphs are $\gamma_A = \gamma_C = 0.077207219973$ and $\gamma_B = 0.082508095136$. The physical dimension of the subgraph is $5^{12} = 244\,140\,625$, which is reduced further (by projection to the virtual degrees of freedom) to $16 \times 27 \times 25 \times 27 \times 16 = 4\,665\,600$. Using the method described in Sec. II G 2, the lower bound of the subgraph gap is calculated to be $\gamma_0 = 0.058117906479$.

Combining the above results, we have a lower bound on the gap of the AKLT Hamiltonian on the inscribed square lattice of

$$\begin{aligned}\Delta_{\text{lower}} &= \gamma_0(1 - \tilde{z}\eta) \\ &= 0.010419962243. \end{aligned} \tag{35}$$

IV. CONSIDERATIONS FOR THE KAGOME AND SQUARE LATTICES

A. Attempts on the kagome lattice

We choose the subgraph Γ as in Fig. 11. Each Γ_i overlaps with $\tilde{z} = 6$ other Γ_j's with the same configuration. The total virtual dimension $U_L \otimes U_M \otimes U_R$ acts on is $324 \times 27 \times 324 = 2\,834\,352$. The resulting overlap parameter is $\eta = 0.17067852083 > \frac{1}{6}$, which does not satisfy the gap criterion unfortunately. So with this overlapping scheme we cannot prove the existence of a gap in the kagome AKLT model, although this does not imply that the gap does not exist.

Noting that η just slightly exceeds the threshold, we naturally guess that by using a larger subgraph partition, we might be able to find an η which satisfies the criteria. Here we propose another overlapping scheme shown in Fig. 12. For each subgraph, there are six others that overlap it, and these overlapping pairs are divided into 2 types, as some of the pairs are topologically identical. The total virtual dimensions $U_L \otimes U_M \otimes U_R$ acts on are $8748 \times 27 \times 8748 = 2\,066\,242\,608$ and $8748 \times 729 \times 3888 = 24\,794\,911\,296$ for the two different pairs. Unfortunately, these dimensions are too large for our current computing resources.

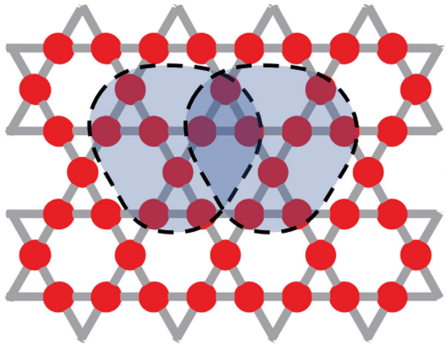

FIG. 11. The kagome lattice and an overlapping scheme that has been tested.

B. A possible attempt on the square lattice

Here we present an overlapping scheme for the square lattice; see Fig. 13. Each subgraph overlaps with $\tilde{z} = 8$ neighboring subgraphs. The overlapping pairs can be divided into 2 types: AB (4 pairs) and AC (4 pairs), with respective virtual dimension $2916 \times 6561 \times 2916 = 55\,788\,550\,416$ and $78732 \times 81 \times 78732 = 502\,096\,953\,744$. If we could prove that $4\eta_{AB} + 4\eta_{AC} < 1$, then we could prove the existence of a spectral gap in the square lattice AKLT model. However, these dimensions are too large for us to carry out the calculations.

V. A FINITE-SIZE CRITERION FOR THE SQUARE-LATTICE MODEL

Here we prove a finite-size criterion, inspired by the work of Lemm, Sandvik and Wang [18] on the hexagonal lattice. To do this, we select an $N \times N$ region with $4N$ additional sites around it, as shown in Fig. 14, and a factor a to weight Hamiltonian terms by. We find that the original AKLT gap in the thermodynamic limit can be bounded by the following

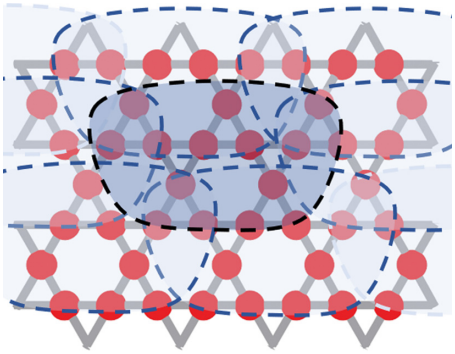

FIG. 12. Another kagome lattice overlapping scheme.

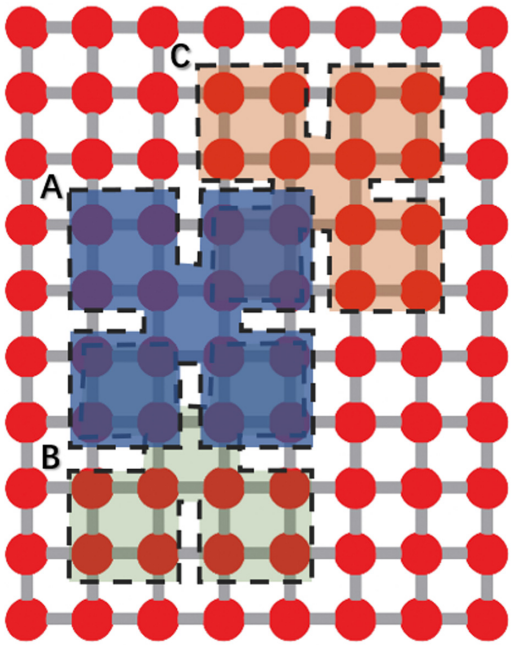

FIG. 13. A proposed overlapping scheme for the square lattice. There are two types of overlapping pairs: AB and AC. We suspect the partition presented here could be used to prove the existence of the gap of the spin-2 square-lattice AKLT model. However, its computational cost is still out of reach given present resources.

expression:

$$\Delta \geqslant \frac{f(a)}{g(a)}\left(\gamma_F(a) - \frac{f(a^2)-g(a)}{f(a)}\right), \tag{36}$$

where

$$f(a) \equiv 2(2N-1) + (N-1)(N-2)a, \tag{37}$$

$$g(a) \equiv 2N + 2(N-2)a + (N-2)^2a^2, \tag{38}$$

and $\gamma_F(a)$ is the actual gap of the weighted finite-size AKLT Hamiltonian on the subgraph. By fine-tuning the parameter a we might find that the actual finite-size gap $\gamma_F(a)$ exceeds the threshold $\gamma_{\rm TH}(a) \equiv \frac{f(a^2)-g(a)}{f(a)}$, making the lower bound a positive value. If so, this would prove the existence of the spectral gap for the original AKLT model on the square lattice. The minimum $\gamma_{\rm TH}$'s for subgraphs with different sizes N (i.e., the feature length) are shown in Table I.

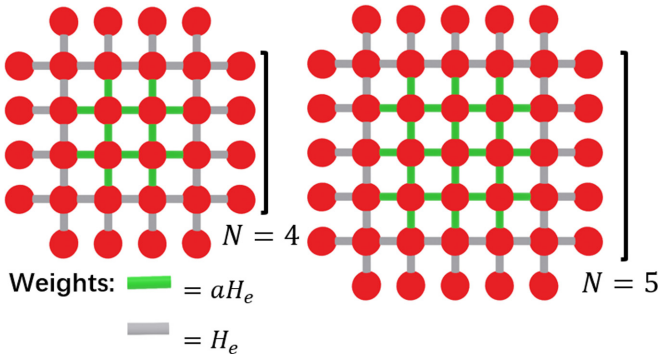

FIG. 14. An illustration of the subgraph $\mathcal{F}_\square$, with $N \times N$ plaquettes and $4N$ surrounding sites. We note that $N \geqslant 3$, and two examples with $N = 4$ and $N = 5$ are shown.

TABLE I. Threshold $\gamma_{\rm TH}$ of the subgraph gap lower bound in order to establish the gap in the thermodynamic limit for the square-lattice AKLT model.

N	a	$\gamma_{\rm TH}$
4	1.28759	0.191729
5	1.31366	0.156829
10	1.3654	0.081199
20	1.39034	0.0410889
40	1.40244	0.0206377
100	1.40954	0.00827357

In fact, by examining its dependence on N, we observe that $\gamma_{\rm TH} \sim O(\frac{1}{N})$. We expect that, as N increases, γ_F will converge to $a\Delta$, and so with N large enough it should exceed the threshold, hopefully while the problem size is numerically accessible. In Appendix B, we give details of the proof for the finite-size criterion; we illustrate different types of pairs of projectors in Fig. 15.

Discussion

For a subgraph with size N and interior edge weight a, we can prove that the infinite lattice is gapped if the gap is greater than $\gamma_{\rm TH}(a)$, where

$$\gamma_{\rm TH}(a) = \frac{(N-2)a^2 - 2(N-2)a + 2(N-1)}{(N-1)(N-2)a + 2(2N-1)}. \tag{39}$$

The behavior of $\gamma_{\rm TH}(a)$ is shown in Fig. 16 for a few N's and the minimum values are tabulated in Table I.

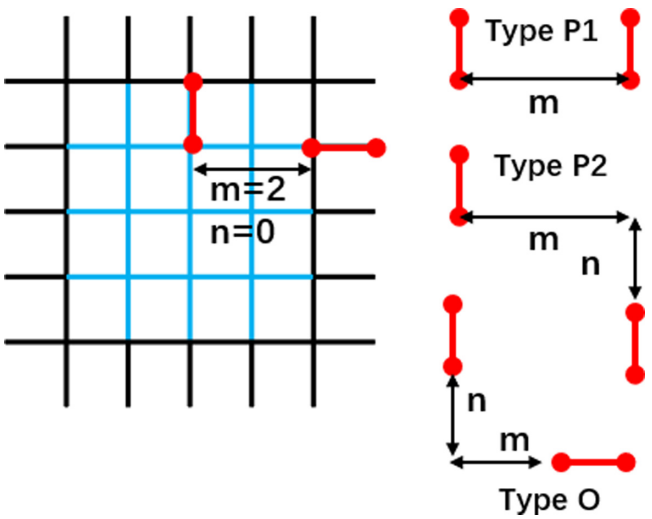

FIG. 15. Illustration of the subgraph $\mathcal{F}_\square$ (left) and three types of edge pairs (right). To analyze the R term in Eq. (B10a), we categorize pairs of edges into three types. The accumulated weight of each type of pair is summarized in Tables II, III, and IV, respectively. An example pair of type **O**, with $m = 2$, $n = 0$ and weight $a \times 1 = a$, is shown in a $N = 5$ subgraph.

TABLE II. The accumulated weights of type **P1** edge pairs in an $N \times N$ subgraph. Note that the case of $m = 0$ is excluded, as it counts terms in $\tilde{H}_{\mathcal{F}_\square}$ and gives $f(a^2)$. It is straightforward to check that all entries in the right column are not greater than $g(a) = 2N + 2(N-2)a + (N-2)^2a^2$.

m	$h_i(a)$
$1 \leqslant m \leqslant N-2$	$2(N-m) + 2(N-1)a + (N-1)(N-2-m)a^2$
$N-1$	$N+1$

One can analytically find the minimal value of $\gamma_{\rm TH}$:

$$a_0 \equiv \arg\min_a(\gamma_{\rm TH}(a)) = \frac{-4N+2+\sqrt{2N^4-2N^3+6N^2-2N}}{(N-1)(N-2)}, \quad (40a)$$

$$\gamma_{\rm TH}(a_0) = -2\frac{N^2+N-\sqrt{2N^4-2N^3+6N^2-2N}}{(N-1)^2(N-2)}. \quad (40b)$$

In the large N limit, $\gamma_{\rm TH}$ is inversely proportional to N,

$$a_0 = \sqrt{2} + \mathcal{O}\left(\frac{1}{N}\right), \quad (41a)$$

$$\gamma_{\rm TH}(a_0) = \frac{2\sqrt{2}-2}{N} + \mathcal{O}\left(\frac{1}{N^2}\right). \quad (41b)$$

We note that the scaling in Eq. (41b) slightly improves the result of $3/N$ by Lemm [23]. We note that it should be possible to allow more weights in the Hamiltonian to improve the threshold to be inversely proportional to the square of the linear size [24–27].

In the large a limit, $\gamma_{\rm TH}$ is linear in a as expected and inversely proportional to N:

$$\gamma_{\rm TH} = \frac{1}{N-1}a + \mathcal{O}(1). \quad (42)$$

If the infinite lattice has a gap Δ, one would expect, as one increases N, the boundary effect diminishes and the subgraph gap γ_F converges to $a\Delta$. However, one can make the gap threshold $\gamma_{\rm TH} \sim \mathcal{O}(\frac{1}{N})$ arbitrary small. Therefore, with a large enough N, one should be able to find a configuration where the gap is greater than the threshold, which would prove the existence of the gap.

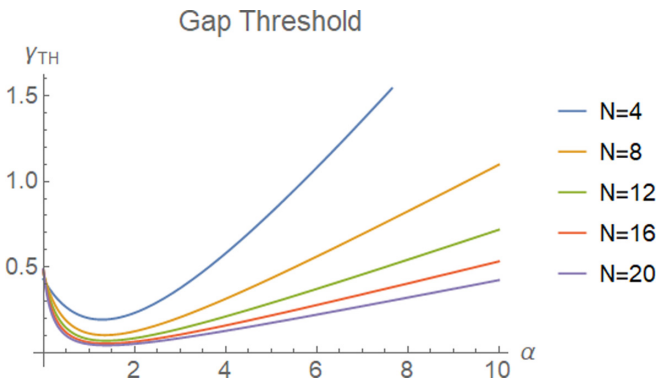

FIG. 16. The gap threshold $\gamma_{\rm TH}(a)$ for a few finite sizes N.

In contrast, if the infinite lattice is gapless, then one would expect that the gap γ_F of a finite-size subgraph would converge to zero as N increases, and $\gamma_{\rm TH}$ would provide an upper bound for the diminishing gap. However, it is strongly believed that the AKLT model on the square lattice is gapped, as provided by the exponential decay of the two-point correlation function [22]. Two estimates of the gap in the thermodynamic limit using numerical tensor-network methods give a consistent value of $\Delta \approx 0.015$ [28,29]. Further strong evidence of the existence of the gap on the square lattice was obtained from studying the boundary state of the model [30].

VI. CONCLUDING REMARKS

We have established the existence of nonzero spectral gap for AKLT models on five lattices: (1) the singly decorated diamond lattice; (2) two singly decorated kagome lattices; (3) the triangle-octagon lattice, where an octagon is inserted into each plaquette, creating four triangles surrounding each site of the original square lattice; (4) the "inscribed" square lattice, where a diamond (or alternatively circle) is inscribed in every other plaquette of the square lattice. The first three models in (1) and (2) are composed of a mixture of spin-2 and spin-1 degrees of freedom. The spin-2 model on the undecorated diamond lattice is known to be magnetically disordered, but the existence of a gap is still an open question. The consideration of the decorated diamond lattice may be regarded as an analysis of a nontrivial three-dimensional model by itself and a step towards solving the undecorated model. Intuitively, decorating the diamond lattice with a spin-1 degree of freedom on every edge introduces more quantum fluctuation (than in the original diamond lattice) and reduces the tendency towards magnetic ordering. The unique ground state and the proof of a gap for the decorated diamond lattice support this intuition. In addition to its existence, we also provide different approaches to lower bound the value of the gap, though we believe that values we obtained are much smaller than the actual gap.

AKLT models on all 2D regular lattices are disordered [21]. The kagome lattice has geometric frustration, whose effect is subtly reflected by certain generalized measurements [14,15]. However, decoration by introducing spin-1 sites reduces this frustration. We have shown that the AKLT models on two decorated kagome lattices are also gapped. The other two planar models we considered derive from modification of the square lattice and both consist of uniformly spin-2 degrees of freedom. To our knowledge, these are the only spin-2 AKLT models for which a gap has been proven. In the square and kagome lattice models, the gap is believed to exist but still has not been proven.

We have also made an attempt on the kagome case and have selected the lattice partition in Fig. 11, where $\tilde{z} = 6$. The η parameter for such a configuration was calculated to be $\eta \approx 0.1707 > 1/6$. Unfortunately, this value just barely exceeds $1/\tilde{z}$ by less than 3% and a nonzero gap cannot be concluded. One thus needs to consider a partition with larger unit cells, such as the one shown in Fig. 12. However, the problem size for that is beyond our current numerical capacity.

For the square lattice, we also suggest a partition in Fig. 13 that might be used to test the gap criterion for the square-lattice AKLT model. However, the computer memory needed

TABLE III. The accumulated weights of type **P2** edge pairs in an $N \times N$ subgraph. The case $m = n = 0$ is excluded as it counts terms in $Q_{\mathcal{F}_\square}$ and gives $g(a)$. (Note further that n counts the *edges between* the two in question, not the total offset, which is why, e.g., the case $m = n = 0$ is edges that are *touching* rather than fully coinciding.) It is straightforward to check that all entries in the last column are not greater than $g(a) = 2N + 2(N-2)a + (N-2)^2a^2$.

m	n	$h_i(a)$
0	$1 \leqslant n \leqslant N-2$	$2(N-n) + 2(N-2)a + (N-2)(N-2-n)a^2$
$1 \leqslant m \leqslant N-2$	$0 \leqslant n \leqslant N-2$	$2 + 2(2N-3-m-n)a + (N-2-m)(N-2-n)a^2$
$N-1$	$0 \leqslant n \leqslant N-2$	$N-n$
0	$N-1$	N
$1 \leqslant m \leqslant N-2$	$N-1$	$N-m$
$N-1$	$N-1$	1

to perform the calculation is also beyond our capacity. As another approach, we have derived a finite-size criterion for the square lattice similar to the one of Lemm, Sandvik and Wang for the hexagonal lattice [18]. If we take the previously estimated thermodynamic gap $\Delta \approx 0.015$ as the target, we would need to take $N = 40$ in order for $\gamma_{\mathrm{TH}}(a_0)/a_0$, i.e. the local gap threshold divided by the local Hamiltonian weight a_0, to fall below the value 0.015. Numerical estimation of the local gap for such a large problem size may be inaccessible. Nevertheless, the scaling is likely to be improved [24–27] and a lower value of N might suffice. In conclusion, establishing rigorously the existence of the nonzero gap in the AKLT model on the square lattice remains open.

ACKNOWLEDGMENT

This work was supported by the National Science Foundation under Grant No. PHY 1915165.

APPENDIX A: DIFFERENT LOWER-BOUNDING METHODS FOR THE SINGLY DECORATED DIAMOND LATTICE

In calculating the gap bound for the decorated diamond lattice we have five results coming from three different intermediate Hamiltonians. The results here are presented with fewer digits of precision than in the main text.

(1) Five-vertex Hamiltonian terms (a spin-2 plus the four adjacent spin-1s), as in Fig. 8: $H^5 = \frac{1}{4}(H_A^5 + H_B^5 + H_C^5 + H_D^5) + H_E^5$. The H_X^5 are bounded relative to the original Hamiltonian by $\gamma_5 = 0.1706462$, and the bound of H_5 relative to the full 17-vertex projector is $\gamma_R = 0.1583008$, giving an overall relative bound of $\gamma_0 = 0.02701344$.

(2) Six-vertex Hamiltonian terms (an outer spin-2 and the four surrounding spin-1s plus the inner spin-2), as in Fig. 9: $H^6 = H_A^6 + H_B^6 + H_C^6 + H_D^6$, where we have to bound H_X^6 relative to sum of terms from the original Hamiltonian where (unlike in the other cases where all coefficients are 1) the four terms that include the outer spin-2 have coefficient 1/4; this gives $\gamma_6' = 0.04437436$.

(a) By computing the overlap parameter $\eta' = 0.2348484\ldots$ (between projectors of the two overlapping regions) we get the relative bound $\gamma_0 = 0.01311061$.

(b) Alternatively, by using proportion 5 of the SM of Ref. [17] we bound H^6 relative to the full projector with $\gamma_R = 0.3274050$, getting $\gamma_0 = 0.01452839$.

(3) Nine-vertex Hamiltonian terms (an outer spin-2 and the central spin-2 plus the 7 spin-1s neighboring either), as in Fig. 17: $H^9 = \frac{1}{4}(H_A^9 + H_B^9 + H_C^9 + H_D^9)$.

(a) The H_X^9's are bounded relative to the original Hamiltonian by $\gamma_9 = 0.02066720$. By computing the overlap $\eta' = 0.05060345$ we get the relative bound $\gamma_0 = 0.01752971$.

(b) Alternatively, by using proposition 5, we bound H^9 relative to the full projector with $\gamma_R = 0.8655232$, getting $\gamma_0 = 0.01788794$.

All of the above five different values of γ_0 give respective lower bounds on the AKLT gap via $\Delta_{\mathrm{lower}} = \gamma_0(1 - \tilde{z}\eta)$, where $\tilde{z} = 12$ and $\eta = 0.041310153882$ was obtained in Sec. III A.

APPENDIX B: PROOF DETAILS FOR THE SQUARE-LATTICE FINITE-SIZE CRITERION

We use $\mathcal{F}_\square$ to denote an instance of the weighted graph $\mathcal{F}$ as a subgraph of the lattice Λ in Fig. 14, which consists of

TABLE IV. The accumulated weights of type **O** edge pairs in an $N \times N$ subgraph. Note that m and n are exchanged by reflections across $x = y$, so the table is symmetric under exchange of m and n. The case $m = n = 0$ is excluded as it counts terms in $Q_{\mathcal{F}_\square}$ and will give $g(a)$. It is straightforward to check that all entries in the right column are not greater than $g(a) = 2N + 2(N-2)a + (N-2)^2a^2$.

m	n	$h_i(a)$
0	$1 \leqslant n \leqslant N-2$	$(N+1-n) + (3N-5-n)a + (N-2)(N-2-n)a^2$
0	$N-1$	N
$1 \leqslant m \leqslant N-2$	$1 \leqslant n \leqslant N-2$	$2 + 2(2N-3-m-n)a + (N-2-n)(N-2-m)a^2$
$1 \leqslant m \leqslant N-2$	$N-1$	$N-m$
$N-1$	$1 \leqslant n \leqslant N-2$	$N-n$
$N-1$	$N-1$	1

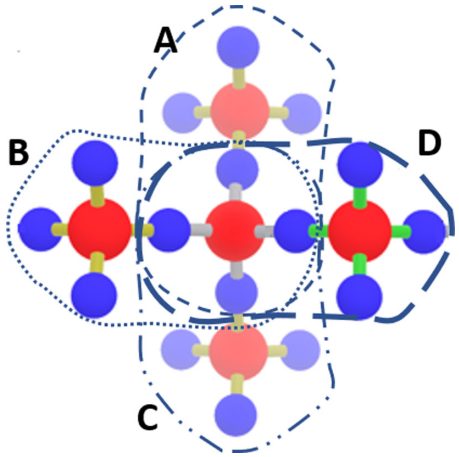

FIG. 17. Partitioning the subgraph into four overlapping regions, each with 9 spins.

$N \times N$ plaquettes at the center, including a central plaquette $\square \in \Lambda$, and $4N$ surrounding 'dangling' sites connecting to it. The edge set of $\mathcal{F}_\square$ is denoted by $\mathcal{E}_{\mathcal{F}_\square}$.

To each translation of $\mathcal{F}_\square$, indexed by all plaquettes $\square$, we assign an operator $H_{\mathcal{F}_\square} = \sum_{e\in\mathcal{E}_{\mathcal{F}_\square}} w_e P_e$, where P_e is the AKLT Hamiltonian term (a projector) on two neighboring spins connected by an edge e and the weight w_e is either 1 or a, according to the pattern indicated in Fig. 14. We then square $H_{\mathcal{F}_\square}$ and sum over all translations (of the plaquette $\square$),

$$\mathcal{A} \equiv \sum_{\square\in\Lambda} H_{\mathcal{F}_\square}^2. \tag{B1}$$

There are two operator inequalities that we will derive, following the idea in Ref. [18]:

$$\mathcal{A} \geqslant f(a)\gamma_{\mathcal{F}} H, \tag{B2}$$

$$\mathcal{A} \leqslant f(a^2)H + g(a)(Q+R), \tag{B3}$$

where f and g are two functions defined below, H is the original AKLT Hamiltonian on the whole lattice Λ, and Q and R contain terms involving pairs of edges in H^2 which share a vertex or not, respectively:

$$H = \sum_{e\in\mathcal{E}} P_e, \tag{B4}$$

$$Q = \sum_{e,e'\in\mathcal{E}, e\sim e'} \{P_e, P_{e'}\}, \tag{B5}$$

$$R = \sum_{e,e'\in\mathcal{E}, e\nsim e'} \{P_e, P_{e'}\}. \tag{B6}$$

After we square the total Hamiltonian H, the squared terms give back H and there are two types of cross-terms, such that

$$H^2 = H + Q + R. \tag{B7}$$

By combining Eqs. (B2) and (B3), derived below, we conclude that

$$H^2 \geqslant \frac{f(a)}{g(a)}\left(\gamma_F(a) - \frac{f(a^2)-g(a)}{f(a)}\right)H, \tag{B8}$$

and hence the lower bound in Eq. (36), provided the expression inside the bracket in Eq. (B8) is positive.

Proof of Eqs. (B2) and (B3). We first study the number of single-edge terms in $\sum_{\square\in\Lambda} H_{\mathcal{F}_\square}$. There are two equivalent types of edges, vertical and horizontal edges, each of which appears, in $\mathcal{F}_\square$, $(N-1)(N-2)$ times within the central square and $2(2N-1)$ times outside of it. Thus, by translation, the accumulated weight for each edge term is $f(a) = 2(2N-1) + (N-1)(N-2)a$. If we label the gap of $H_{\mathcal{F}_\square}$ as $\gamma_{\mathcal{F}}$, then we can lower-bound $\mathcal{A}$ as

$$\mathcal{A} = \sum_{\square\in\Lambda} H_{\mathcal{F}_\square}^2 \geqslant \sum_{\square\in\Lambda} \gamma_{\mathcal{F}} H_{\mathcal{F}_\square} = \gamma_{\mathcal{F}} f(a) H. \tag{B9}$$

We then consider the number of cross-terms in $\mathcal{A} = \sum_{\square\in\Lambda} H_{\mathcal{F}_\square}^2$ and decompose $H_{\mathcal{F}_\square}^2 = \tilde{H}_{\mathcal{F}_\square} + Q_{\mathcal{F}_\square} + R_{\mathcal{F}_\square}$, where

$$\tilde{H}_{\mathcal{F}_\square} = \sum_{e\in\mathcal{E}_{\mathcal{F}_\square}} w_e^2 P_e, \tag{B10a}$$

$$Q_{\mathcal{F}_\square} = \sum_{e,e'\in\mathcal{E}_{\mathcal{F}_\square}, e\sim e'} w_e w_{e'} \{P_e, P_{e'}\}, \tag{B10b}$$

$$R_{\mathcal{F}_\square} = \sum_{e,e'\in\mathcal{E}_{\mathcal{F}_\square}, e\nsim e'} w_e w_{e'} \{P_e, P_{e'}\}. \tag{B10c}$$

Since each cross-term only arises when both edges are in the same subgraph $\mathcal{F}_\square$, we expect we can use constant coefficients to bound $Q_{\mathcal{F}_\square}$ and $R_{\mathcal{F}_\square}$ relative to Q and R.

As the weight of each edge in $\tilde{H}_{\mathcal{F}_\square}$ is squared, we straightforwardly determine that the coefficient (which we also call the "accumulated weight") for each edge in $\mathcal{A}$ is $f(a^2)$:

$$\sum_{\square\in\Lambda} \tilde{H}_{\mathcal{F}_\square} = f(a^2) H. \tag{B11}$$

For each pair of edges which share one vertex, one can easily see by counting that both the parallel and perpendicular cases have the same accumulated weight $g(a) \equiv 2N + 2(N-2)a + (N-2)^2 a^2$, and thus

$$\sum_{\square\in\Lambda} Q_{\mathcal{F}_\square} = g(a) Q. \tag{B12}$$

It turns out that the number of combinations of edges in each class of R can be bounded by those of Q. There are three types of equivalent classes of pairs:

P1: a pair of parallel edges separated by m edges along the direction perpendicular to them.

P2: a pair of parallel edges separated by m edges in the parallel and n in the perpendicular direction.

O: a pair of orthogonal edges separated by m edges parallel to the first one and n edges parallel to the second.

See Fig. 15 for an illustration of these three classes. We tabulate all possible cases i of the accumulated weight $h_i(a)$ in these three classes in Tables II–IV. As can be checked, for $N \geqslant 4$ all cases are less than or equal to $g(a)$ for positive a, so we conclude that

$$\sum_{\square\in\Lambda} R_{\mathcal{F}_\square} \leqslant g(a) R. \tag{B13}$$

Summing up, we arrive at Eq. (B3).

[1] I. Affleck, T. Kennedy, E. H. Lieb, and H. Tasaki, Rigorous Results on Valence-Bond Ground States in Antiferromagnets, Phys. Rev. Lett. **59**, 799 (1987).

[2] I. Affleck, T. Kennedy, E. H. Lieb, and H. Tasaki, Valence bond ground states in isotropic quantum antiferromagnets, Commun. Math. Phys. **115**, 477 (1988).

[3] Z.-C. Gu and X.-G. Wen, Tensor-entanglement-filtering renormalization approach and symmetry protected topological order, Phys. Rev. B **80**, 155131 (2009).

[4] F. Pollmann, E. Berg, A. M. Turner, and M. Oshikawa, Symmetry protection of topological order in one-dimensional quantum spin systems, Phys. Rev. B **85**, 075125 (2012).

[5] X. Chen, Z.-C. Gu, Z.-X. Liu, and X.-G. Wen, Symmetry-protected topological orders in interacting bosonic systems, Science **338**, 1604 (2012).

[6] F. D. M. Haldane, Continuum dynamics of the 1-D Heisenberg antiferromagnet: Identification with the O(3) nonlinear sigma model, Phys. Lett. **93**, 464 (1983).

[7] F. D. M. Haldane, Nonlinear Field Theory of Large-Spin Heisenberg Antiferromagnets: Semiclassically Quantized Solutions of the One-Dimensional Easy-Axis Neel State, Phys. Rev. Lett. **50**, 1153 (1983).

[8] S. Knabe, Energy gaps and elementary excitations for certain VBS-quantum antiferromagnets, J. Stat. Phys. **52**, 627 (1988).

[9] M. Fannes, B. Nachtergaele, R. F. Werner, Finitely correlated states on quantum spin chains, Commun. Math. Phys. **144**, 443 (1992).

[10] D. Gross and J. Eisert, Novel Schemes for Measurement-Based Quantum Computation, Phys. Rev. Lett. **98**, 220503 (2007).

[11] G. K. Brennen and A. Miyake, Measurement-Based Quantum Computer in the Gapped Ground State of a Two-Body Hamiltonian, Phys. Rev. Lett. **101**, 010502 (2008).

[12] T.-C. Wei, I. Affleck, and R. Raussendorf, Affleck-Kennedy-Lieb-Tasaki State on a Honeycomb Lattice is a Universal Quantum Computational Resource, Phys. Rev. Lett. **106**, 070501 (2011).

[13] A. Miyake, Quantum computational capability of a two-dimensional valence bond solid phase, Ann. Phys. (Leipzig) **326**, 1656 (2011).

[14] T.-C. Wei, Quantum computational universality of spin-3/2 Affleck-Kennedy-Lieb-Tasaki states beyond the honeycomb lattice, Phys. Rev. A **88**, 062307 (2013)

[15] T.-C. Wei, P. Haghnegahdar, and R. Raussendorf, Hybrid valence-bond states for universal quantum computation, Phys. Rev. A **90**, 042333 (2014).

[16] T.-C. Wei and R. Raussendorf, Universal measurement-based quantum computation with spin-2 Affleck-Kennedy-Lieb-Tasaki states, Phys. Rev A **92**, 012310 (2015).

[17] N. Pomata and T.-C. Wei, Demonstrating the Affleck-Kennedy-Lieb-Tasaki Spectral Gap on 2D Degree-3 Lattices, Phys. Rev. Lett. **124**, 177203 (2020).

[18] M. Lemm, A. W. Sandvik, and L. Wang, Existence of a Spectral Gap in the Affleck-Kennedy-Lieb-Tasaki Model on the Hexagonal Lattice, Phys. Rev. Lett. **124**, 177204 (2020).

[19] H. Abdul-Rahman, M. Lemm, A. Lucia, B. Nachtergaele, and A. Young, A class of two-dimensional AKLT models with a gap, in *Analytic Trends in Mathematical Physics*, edited by H. Abdul-Rahman, R. Sims, and A. Young, Contemporary Mathematics Vol. 741 (American Mathematical Society, Providence, RI, 2020), pp. 1–21.

[20] N. Pomata and T.-C. Wei, AKLT models on decorated square lattices are gapped, Phys. Rev. B **100**, 094429 (2019).

[21] S. A. Parameswaran, S. L. Sondhi, and D. P. Arovas, Order and disorder in AKLT antiferromagnets in three dimensions, Phys. Rev. B **79**, 024408 (2009).

[22] T. Kennedy, E. H. Lieb, and H. Tasaki, A two-dimensional isotropic quantum antiferromagnet with unique disordered ground state, J. Stat. Phys. **53**, 383 (1988).

[23] M. Lemm, Finite-size criteria for spectral gaps in D-dimensional quantum spin systems, Contemp. Math. **741**, 121 (2020).

[24] D. Gosset and E. Mozgunov, Local gap threshold for frustration-free spin systems, J. Math. Phys. **57**, 091901 (2016).

[25] M. Lemm and E. Mozgunov, Spectral gaps of frustration-free spin systems with boundary, J. Math. Phys. **60**, 051901 (2019).

[26] A. Anshu, Improved local spectral gap thresholds for lattices of finite size, Phys. Rev. B **101**, 165104 (2020).

[27] M. Lemm (private communication).

[28] A. Garcia-Saez, V. Murg, and T.-C. Wei, Spectral gaps of Affleck-Kennedy-Lieb-Tasaki Hamiltonians using tensor network methods, Phys. Rev. B **88**, 245118 (2013).

[29] L. Vanderstraeten, M. Mariën, F. Verstraete, and J. Haegeman, Excitations and the tangent space of projected entangled-pair states, Phys. Rev. B **92**, 201111(R) (2015).

[30] J. Martyn, K. Kato, and A. Lucia, Deformations of the boundary theory of the square-lattice AKLT model, Phys. Rev. B **102**, 035121 (2020).